Thermal equation of state of F-bearing superhydrous phase B ($Mg_{10}Si_3O_{14}(OH,F)_4$): Implications for the transportation of fluorine and water into Earth's lower mantle

Authors: Xiang Li[1], Yungui Liu[1,2], Ran Wang[3], Takashi Yoshino[3], Jingui Xu[4], Dongzhou Zhang[4], Tobias Grützner[5], Junfeng Zhang[1], Xiang Wu[1*]

Affiliation:

[1]State Key Laboratory of Geological Processes and Mineral Resources, China University of Geosciences (Wuhan), Wuhan 430074, China.

[2]College of Gems and Materials Technology, Hebei GEO University, Shijiazhuang 050031, China.

[3]Institute for Planetary Materials, Okayama University, Misasa, Tottori 682-0193, Japan.

[4]School of Ocean and Earth Science and Technology, Hawai'i Institute of Geophysics and Planetology, University of Hawai'i at Manoa, Honolulu 96822, HI, USA.

[5]Institut de minéralogie, de physique des matériaux et de cosmochimie, Sorbonne Université, 4, Place Jussieu - BC 115 - 75252 Paris Cedex 5, France.

Corresponding author: Xiang Wu (wuxiang@cug.edu.cn)

Key Points:

- No phase transition occurs in F-bearing Shy-B up to 27 GPa and 750 K.
- F component can largely increase the incompressibility, density and bulk velocity of Shy-B.
- Shy-B is an essential carrier to transport F from upper mantle to lower mantle.

Keywords:

F-bearing Shy-B, thermal equation of state, elasticity, water

Abstract

To explore the influence of fluorine (F) on mantle minerals and its behaviors during subducting, we investigated the compressibility of F-bearing superhydrous phase B (Shy-B) using synchrotron-based single-crystal X-ray diffraction combined with diamond anvil cells up to 27 GPa and 750 K. Our results show that the presence of F can largely enhance the incompressibility of Shy-B. Based on the obtained thermal elastic parameters, density and velocity profiles are evaluated along cold and warm slabs. Our results demonstrate that addition of F enhances the density (~1.3-1.7%) and the bulk velocity (~1.0-2.4%) of Shy-B relative to OH end-member at uppermost lower mantle conditions. The decomposition of F-bearing Shy-B would lead to an abrupt increase in density (~8.9-10.5%) and a small increase in bulk velocity (~0.7-1.8%). The combined results could provide constraints for modeling the geodynamic process related to subduction and transportation of F and OH into lower mantle.

Plain Language Summary:

Fluorine is the most abundant halogen in the Earth's mantle. High-pressure and high-temperature experiments show that bridgmanite, the major minerals in lower mantle, can incorporate significate amount of F, indicating that lower mantle may be a potential reservoir for F. Subduction zones are supposed to deliver F and H to deep Earth. Superhydrous phase B, an important hydrous magnesium silicate in subduction zones, plays a key role in the transportation of H from upper mantle to lower mantle, while it may be also a potential carrier of F, since the similar radius between F^- and OH^-. Here, we investigated the influence of F on the compressibility of superhydrous phase B, and we found that the presence of F can largely enhance the compressibility of superhydrous phase B. We further propose that the accumulation and decomposition of F-bearing Shy-B is hard to explain velocity anomaly and melting at the uppermost lower mantle.

1. Introduction

Volatiles have strong effects on the fractional crystallization of magmas, viscosity of melts, and rheology of mantle minerals. Therefore, it is essential to study the distribution and cycling mechanisms of volatile elements such as H, C and halogen group (F, Cl, Br and I) in Earth ’s mantle. The deep cycle of H has been extensively studied during last few decades. Previous studies show that major minerals in transition zone (wadsleyite and ringwoodite) can incorporate up to 30000 μg/g water. (e.g. Smyth, 1987; Inoue, 1994; Kohlstedt et al., 1996). While the major upper and lower mantle minerals, olivine and bridgmanite, can accommodate significantly less water. Thus, transition zone provides another perspective for the analysis of mantle convection patterns, namely whole-mantle convection model of "transition zone water-filter" (Bercovici and Karato, 2003). Recently, the behaviors of F in deep earth have been studied seriously due to its similar radius with OH^-. F concentrations in the Mid Ocean Ridge Basalt (MORB) and Oceanic Island Basalt (OIB) range from 16 to 109 μg/g (Schilling et al., 1980; Saal et al., 2002) and from 34 to 76 μg/g (Joachim et al., 2015) respectively, which are both higher than the estimate for bulk silicate Earth (BSE) (25 μg/g: McDonough and Sun, 1995). Therefore, the abundance of F requires minerals to incorporate this element in Earth’s mantle.

High-pressure and high-temperature (HPHT) experiments show that the solubility of F in forsterite (up to 5100 μg/g: Grützner et al., 2017a) at high pressure is higher than that in wadsleyite (1045 μg/g: Grützner et al., 2018) and ringwoodite (1235 μg/g: Roberge et al., 2015). Therefore, fractionation of H and F will occur during subduction, as water enters preferentially into transition zone and F trends to remaining in peridotite of lowermost upper mantle. Yoshino and Jaseem. (2018) reported that the solubility of F in Al-bearing bridgmanite can up to12917 μg/g. Thus, F is likely to partition into bridgmanite rather than ringwoodite, depending on the significant contrast in solubility of F between Al-bearing bridgmanite and transition zone minerals. We suggest that transition zone water-filter may not be an equivalent fluorine-filter (Fig. 1), F is rather stored either above transition zone or below. One

source of F is that F would be transported from Earth's surface into deep mantle by subduction zones, like the cases of H and C. Although F is partially released during dehydration of oceanic crust and degassed through arc volcanism, ~95% of the subducted F is estimated to be transported into deep mantle (Straub and Layne., 2003), and annual global flux is about 9.9–10 × 10^{12} g (John et al., 2011). Most of dominant mantle minerals are nominally F-free and do not contain more than a few thousand μg/g of F. However, a small component of F can significantly affect the properties of minerals, such as pressure-temperature phase stability, elastic properties and electrical conductivity (e.g. Roberge et al., 2015; Grützner et al. 2017b, 2018; Li et al., 2017; Ulian and Valdrè2017).

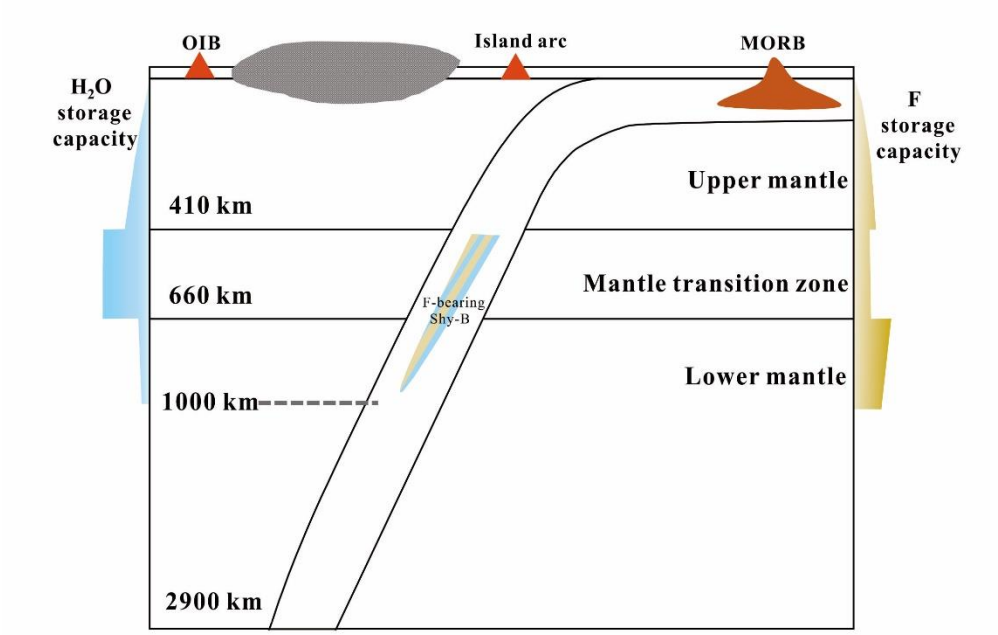

Fig. 1 Schematic model for global fluorine and water storage capacity. At left and right are schematic view of the H_2O and F storage capacity at different depth of Earth's mantle, respectively. We calculated H and F storage capacity in earth mantle using the pyrolite model (Irifune and Ringwood, 1987). Water storage capacity at the bottom of upper mantle can reach up to 10000 μg/g (Hirschmann, 2006). Mantle transition zone can comprise up to 2.5 wt.% (Pearson et al., 2014), and lower mantle can contain 750-4700 μg/g in presence of Al, Fe and F (Yoshino and Jaseem, 2018; Fu et al., 2019). F storage capacity have been calculated for upper mantle (3520 μg/g). The mantle transition zone can store 741-1266 μg/g F and uppermost lower mantle can store 9680 μg/g F. We see a striking difference between behaviors of F and H in Earth's mantle. The "transition zone water-filter" (Bercovici and Karato, 2003) may not be an equivalent fluorine-filter.

Dense hydrous magnesium silicates (DHMSs), important reservoirs for the distribution and transportation of water into deep Earth, are also proposed to be hosts

for F (Hazen et al., 1997). One of the DHMSs, superhydrous phase B (Shy-B) $Mg_{10}Si_3O_{18}H_4$ with 5.8 wt.% H_2O can be stable in mantle transition zone (410 – 660 km) and even down to the uppermost lower mantle (e.g. Inoue et al., 2006; Litasov et al., 2007). It decomposes into phase D, bridgmanite and periclase at around 800 km depth at cold slab conditions and into bridgmanite, periclase and water in hot slabs (e.g. Ohtani et al., 2003). Elasticity and stability of Shy-B have been applied to explain geophysical observations, such as low shear velocity anomalies at the topmost lower mantle and discontinuity at ~800 km discontinuity (Li et al., 2016; Yang et al., 2017). The effects of fluorine should be considered together with those of hydrogen in order to further reveal the natural process of deep Earth. Here, we synthesized two Shy-B samples, OH-rich $Mg_{9.86}Si_{3.14}O_{14}(F_{1.17},OH_{3.11})$ and F-rich $Mg_{9.96}Si_{3.04}O_{14}(F_{2.62},OH_{1.46})$, conducted X-ray single-crystal diffraction (XRD) experiments up to ~ 27 GPa and 750 K, and obtained their equation of state. Based on the results, we discuss the influences of F on mantle minerals, which may have significant implications on the transportation of F from upper to the lower mantle via subduction slabs and for low-velocity zones at uppermost lower mantle.

2. Materials and Methods

2.1. Samples Synthesis and Characterization

High-quality single-crystal OH-rich Shy-B and F-rich Shy-B labeled 5K3408 were synthesized at 20 GPa and 1673 K for around 7 hours using USSA-5000 ton Kawai-type apparatus installed at Institute for Planetary Materials, Okayama University. Two initial samples were placed in single cell and synthesized at same condition. The starting material of OH-rich Shy-B was a mixture of MgO, SiO_2, MgF_2, and $Mg(OH)_2$ with a molar ratio of 8:3:1:1. The starting material of F-rich Shy-B was a mixture of MgO, SiO_2 and MgF_2 with a molar ratio of 8:3:2. The mixture was loaded into an $Au_{80}Pd_{20}$ capsule 2 mm in length and 2 mm in diameter. A Cr-doped MgO octahedron with an edge length of 14 mm was adopted as a pressure medium.

Eight tungsten carbide anvils with a truncation of 6 mm were used as second-stage anvils. For the setup $LaCrO_3$ was used as a heater. The recovered samples are colorless single crystals with small grain size of ~ 200 μm for OH-rich Shy-B and ~ 100 μm for F-rich Shy-B, respectively. Sample characterization were performed at ambient conditions using scanning electron microscope (SEM) equipped with energy dispersive spectrometer (EDS) (Quanta 450 FEG), XRD (Rigaku XtaLAB PRO MM007HF), Raman spectroscopy (Horiba LabRAM HR Evolution) and electron microprobe analysis (EMPA). SEM and EDS results indicated that samples were chemically homogeneous with polyhedral shape (Fig. S1). The measurement conditions for F were those used by Grützner et al. (2017a) and F concentrations in our two samples were determined with a synthetic multi-layered diffraction crystal (LDE). EMPA results show the composition of 61.78 wt% MgO, 29.34 wt% SiO_2 and 3.46 wt% F and 60.68 wt% MgO, 27.66 wt% SiO_2 and 7.53 wt% F for two samples, respectively, yielding the composition of $Mg_{9.86}Si_{3.14}O_{14}(F_{1.17},OH_{3.11})$ labeled OH-rich Shy-B and $Mg_{9.96}Si_{3.04}O_{14}(F_{2.62},OH_{1.46})$ labeled F-rich Shy-B. Their crystal structures are determined to be orthorhombic phase (*Pnnm* and Z=2) with lattice constants of a = 5.0826(2) Å, b = 8.6772(3) Å, c = 13.9911(5) Å, V = 617.05(7) $Å^3$ for OH-rich Shy-B and a = 5.0703(8) Å, b = 8.6729(9) Å, c = 13.8962(4) Å, V = 611.07(11) $Å^3$ for F-rich Shy-B by a micro-focused X-ray diffractometer equipped with Mo $K\alpha$ radiation, respectively. Raman spectra of 16 grains picked randomly are in good agreement with those of Shy-B reported by Liu et al. (2002) (Fig. S2). The results of XRD, Raman spectroscopy, and EMPA demonstrate that the recovered products are pure phases without detectable impurities.

2.2.High-Pressure Synchrotron X-ray Diffraction Experiments

A short symmetry-type diamond anvil cell (DAC) equipped with Böhler-type diamond anvils of 300-μm flat culets anvils was employed to achieve high pressure and 60° opening for room temperature experiments. The sample chamber was formed by drilling a 190-μm-diameter hole in a rhenium gasket that had been pre-indented to ~ 38 μm in thickness. Two single-crystal sample of grain size ~40×40×15 μm^3 were

loaded into sample chamber, as well as a piece of platinum for pressure calibration (Fei et al., 2007). Neon was employed as pressure transmitting medium using the COMPRES/GSECARS gas-loading system. *In situ* high-pressure single-crystal XRD experiments were carried out at beamline 13BM-C at Advanced Photon Source (APS), Argonne National Laboratory (ANL). A monochromatic X-ray beam with wavelength of 0.43409 Å was focused on a 15 × 15 μm^2 spot (Zhang et al., 2017). Wide-scan and stepped exposures were collected in a rotation range from -30° to 30° with 1° steps, with an exposure time of 1 s per frame. Diffraction images were reduced and analyzed using Bruker APEX3 software.

2.3.High pressure-high temperature Synchrotron Radiation XRD Experiments

In situ HPHT single-crystal XRD experiments were conducted up to 26.5 GPa with four different temperatures (300 K, 450 K, 600 K and 750 K) at beamline 13-BMC of APS. A BX90-type DAC equipped with 400-μm flat culets diamond anvils was used combined with an external heater. Two single-crystal samples polished on both sides and with a grain size of~30×30×15 μm^3 were loaded into sample chamber. They were prepared in the same way as the room temperature experiments. Platinum was employed as pressure maker; neon as pressure transmitting medium. As a heater alumina ceramic was coiled by a single platinum wire of 200 μm diameter and ~ 45 cm in length. The measured resistance of heater was ~ 2 Ω. A K-type thermocouple attached close to sample chamber was used to determine temperatures. The GE PACE5000 membrane pressure controller was employed to remotely increase pressure. For each heating run the sample chamber was stabilized for at least 20 minutes at the given temperature to minimize temperature and pressure instability. X-ray diffraction images were collected and analyzed in the same way as the room temperature experiments.

3. Results and Discussion

3.1.Equation of State

In situ high-pressure single-crystal XRD experiments were conducted up to ~27.8 GPa at room temperature. The refined unit-cell parameters of Shy-B at various pressures have been listed in Table S1. The unit-cell volumes of both samples monotonously decrease with increasing pressure, the volumes as a function of pressure are plotted in Fig. 2, where previous relevant data are also plotted for comparison (Shieh et al., 2000; Litasov et al., 2007; Yang et al., 2017). Pressure-volume data were fitted to 2nd-order Birch-Murnaghan (BM) equation of state (EoS) with EoSFit7c (Angel et al., 2014). The fitting results are as follows: V_0 = 615.6(2) Å^3, K_0 = 157(1) GPa for OH-rich sample, V_0 = 610.33(6) Å^3, K_0 = 162(6) GPa for F-rich Shy-B.

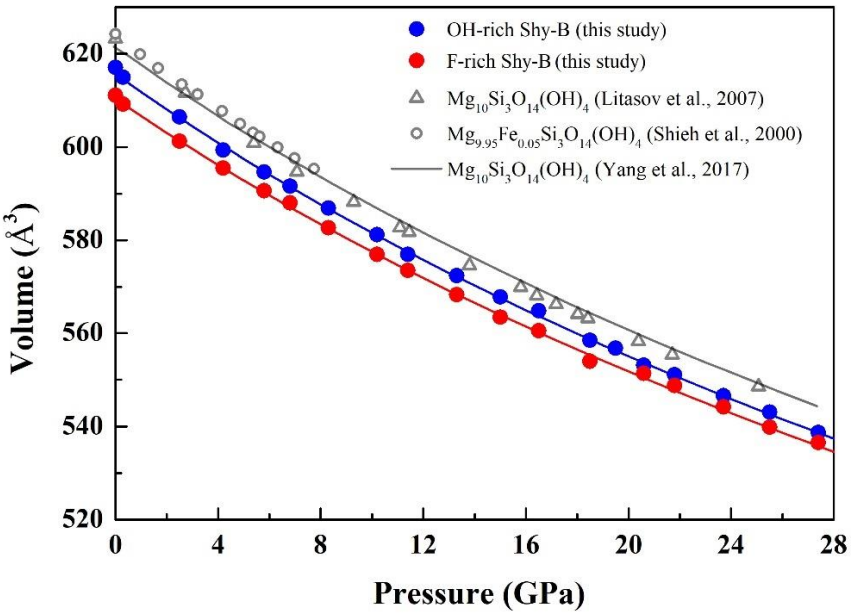

Fig. 2 Unit-cell volumes of F-bearing superhydrous phase B as a function of pressure up to 27.8 GPa. The solid blue and red circles represent OH-rich Shy-B and F-rich Shy-B, respectively. The open gray circles and triangles represent the experimental data from Shieh et al. (2000) and Litasov et al. (2007). The solid gray line represents the results from literature data (Yang et al., 2017). Error bars are smaller than the symbol size for our data.

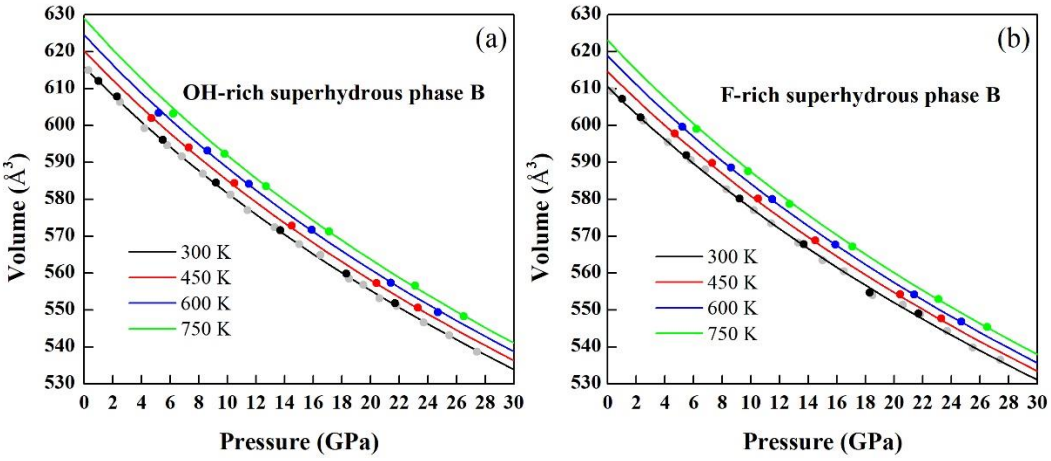

Fig. 3 P-V-T data obtained for (a) OH-rich Shy-B and (b) F-rich Shy-B in this study. The solid lines represent the isothermal compression curves from the high temperature 3rd-order B-M EoS at 300 K, 450 K, 600 K, and 750 K. The gray circles represent the high-pressure experimental data at room temperature in this study.

Fig. 3 shows the unit-cell volumes of two samples at high pressure and high temperature conditions and refined data were presented in Table S2. The experimental data were fitted by B-M thermal EoS (Test S1) up to 26.5 GPa and 750 K (Angel et al., 2014). The thermoelastic parameters are as follows: V_0=615.68(18), K_0=158(7) GPa, $\partial K/\partial T$=-0.020(4) GPa/K, α_0=4.5(2)×10^{-5} K^{-1} for OH-rich Shy-B and V_0= 610.38(7), K_0= 162.4(7) GPa, $\partial K/\partial T$=-0.020(3) GPa/K, α_0= 4.4(1)×10^{-5} K^{-1} for F-rich Shy-B for BM2-EoS. The thermal expansion coefficient of our two samples at atmospheric pressure are significantly larger than previous studies on OH end-member Shy-B with 3.8 ×10^{-5} K^{-1} by Inoue et al. (2006) and 3.2 ×10^{-5} K^{-1} by Litasov et al. (2007).

3.2. Axial Compressibility of F-bearing Shy-B

To investigate the effect of F on axial compressibility of Shy-B, normalized unit-cell lattice parameters (a/a_0, b/b_0 and c/c_0) are plotted for comparison in Fig. S3 with respect to their ambient values for the two F-bearing Shy-B samples. No visible discontinuity was observed in axial compressibility of the both samples up to 27.8 GPa. To determine axial compressibility of *a*, *b*, and *c* of both samples, we used a

linearized 2nd-order BM EoS fitting where each axial dimension is cubed and treated as volume in BM formulation, where the pressure derivatives assumed to be 12. We fitted our linear moduli to a/a_0, b/b_0 and c/c_0 for OH-rich Shy-B are 448(18), 474(19), 477(7) GPa, while for F-rich Shy-B, we obtained linear moduli for a/a_0, b/b_0 and c/c_0 of 507(8), 510(20), and 459(18) GPa. There is no considerable anisotropy in axial compressibility in both phases, which is in good agreement with that of Kudoh et al. (1994), Crichton et al. (1999), Shieh et al. (2000) and Litasov et al. (2007). It is obvious that the OH-rich Shy-B is more compressible than F-rich Shy-B for *a*- and *b*-axis. The axial compressibility of two samples at high *P*-*T* conditions (Fig. S4), shows that temperature has no effects on the axial compressional anisotropy.

3.3.Effects of F on minerals

The volume of Shy-B decreases with increasing F content at ambient conditions (Fig. 1), which is attributed to the smaller ionic radius of F^- (1.31 Å) relative to that of OH^- (1.35 Å). It is obvious that the volume of F-rich Shy-B becomes closer to OH-rich Shy-B with increasing pressure in Fig 1. The isothermal bulk moduli K_0 of Shy-B are summarized in Table S3. We refitted the *P*-*V* data from literature using the 2nd-order BM EoS with a fixed $K' = 4$ for systematic comparison. Bulk modulus K_0 of F-bearing Shy-B (K_0 = 156.9 and 162 GPa) is significantly higher than the results for those of OH end-member Shy-B from Crichton et al. (1999), Inoue et al. (2006) and Litasov et al. (2007) with K_0 = 148.9 (5), 124.8 (3) and 145.2 (4) GPa, indicating that presence of F can increase the K_0 remarkably. The great influences of F on compressibility is in good agreement with previous results from F-bearing minerals. For example, F-bearing chondrodite has a higher bulk modulus than synthetic OH-chondrodite (Kuribayashi et al., 1998; Ross and Crichton, 2001 and references therein) and K_0 of topaz also increases with fluorine content (Ulian and Valdrè, 2017). Therefore, F^- in Shy-B can lead to a higher isothermal bulk modulus. We also report the relationship between the isothermal bulk modulus (K_0) and its pressure derivative (K') of humite minerals and Shy-B to explore the influence of F on compression of those minerals (Fig. S5a). We found that the presence of F would present obvious

crystal-chemical trends, such as enhancing value of K_0 and reducing value of K'. Fig S5b and Table S4 show plots of th bulk modulus against the density of DHMSs, which reveal a positive correlation between K_0 and density.

4. Geophysical Implications

Recently, seismic low velocity zone has been observed at depths of the uppermost lower mantle (Schmandt et al., 2014), which is explained as the result of dehydration melting. Since Shy-B is expected to be a potential carrier of water to uppermost lower mantle, the accumulation and decomposition of Shy-B can help to explain the observed low-velocity layers in this region (Li et al., 2016; Yang et al., 2017). To understand the geophysical and geodynamic significance of our results in a subducting slab, we have evaluated density (ρ) and bulk velocity (V_Φ) profiles of two samples as a function of pressure along both cold and hot slab geotherms (Fig. 4). Our modeled results show that the density of F-bearing Shy-B samples are lower than those of the preliminary reference Earth model (PREM) (Dziewonski and Anderson, 1981), indicating that presence of F-bearing Shy-B can contribute to a positive buoyancy force in subducted slabs at uppermost lower mantle (Fig. 4). Inoue et al. (2006) calculated the density of subducting slabs containing OH end-member Shy-B and discussed that the presence of DHMSs in slabs can affect its ability to penetrate into Earth's lower mantle. The presence of ~18% OH end-member Shy-B at the top of lower mantle would reduce the density of the hydrated subducting slab by 1.9–2.1%. Accordingly, a homogeneously hydrated slab may float at the bottom of transition zone and would not be able to penetrate into deep lower mantle (Litasov et al., 2007). However, our modeled results for OH-rich and F-rich Shy-B are ~1.3% and 1.7% denser than OH end-member Shy-B both under cold and hot slab geotherms, which would enhance the density of hydrated subducting slab by ~0.13 % and ~0.2%, respectively. Due to its lower density relative to the main minerals in lower mantle, F-bearing Shy-B may accumulate at depths of the topmost lower mantle while the

subduction continues. Our results show that addition of F in Shy-B leads to ~1.8% and ~2.4% increase in bulk sound velocity for OH-rich and F-rich Shy-B compared with the OH end-member in cold slab geotherms, respectively. While increases by ~1.0% and ~2.1% for OH-rich and F-rich Shy-B at hot slab geotherms. Hence, it is hard to explain low shear velocity anomalies at uppermost lower mantle by an accumulation of F-bearing Shy-B, which may need much more Shy-B than previous predict (Li et al., 2016).

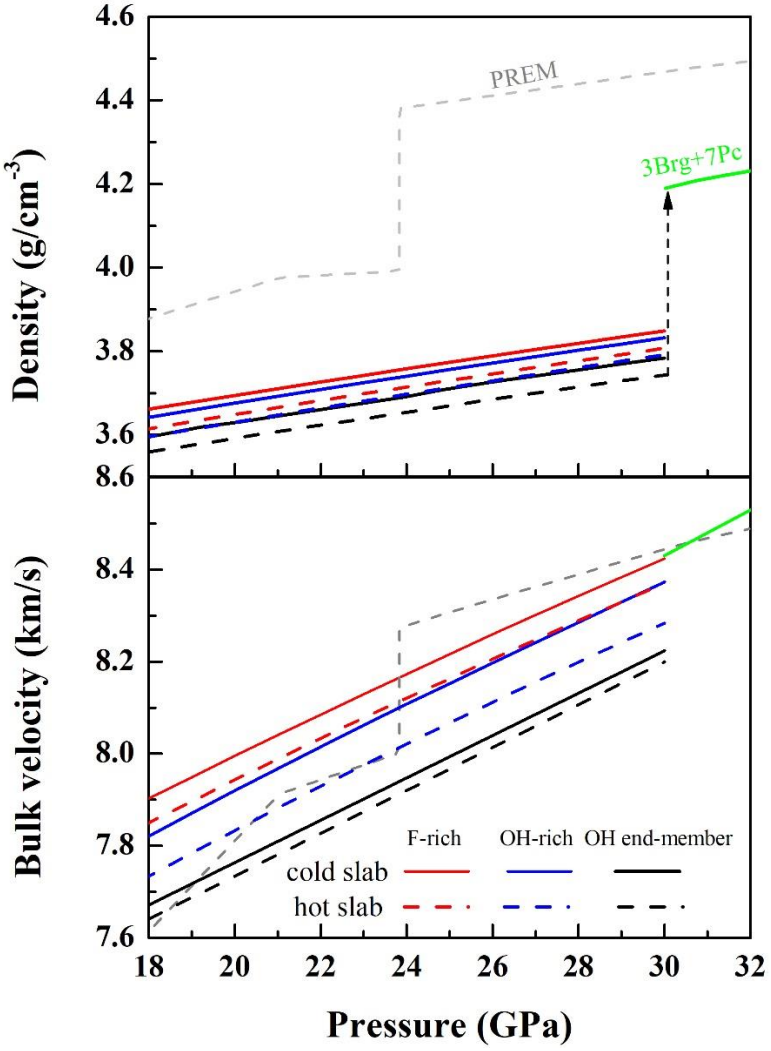

Fig. 4 Density (ρ) and bulk sound velocity (V_Φ) of the two samples which have been compared with the preliminary reference Earth model (PREM) (Dziewonski and Anderson, 1981) and the aggregate of 7 iron-free bridgmanite (Brg) + 3 periclase (Pc) under both cold (900K) and hot (1300K) slabs geotherms.

Shy-B is an important candidate for water transportation into transition zone and lower mantle, which can experience a series of dehydration reactions. It decomposes

stoichiometrically into 3bridgmanite, 7periclase and $2H_2O$ at 800~1000 km depth depending on the temperature of slab. We modeled changes of density (ρ) and bulk sound velocity (V_Φ) across these phases transition (Fig. 4) and we calculated ρ and V_Φ of 3bridgmanite and 7periclase combined with the elastic parameters from Yang et al. (2017). As there are currently no parameters available for F-bearing bridgmanite and periclase, we use the data of F- and OH-free bridgmanite ($MgSiO_3$) and periclase (Yang et al., 2017) as best approximation. Our modeled results show that the decomposition of F-bearing Shy-B leads to a density increase by ~9.3% and ~8.9% for OH-rich and F-rich Shy-B, respectively, along cold slabs, and a density increase by ~10.5% and ~10.1% for OH-rich and F-rich Shy-B along hot slabs at uppermost lower mantle conditions. However, there is only a small V_Φ increase of ~1.8% and ~0.7% along hot subducted slabs. In cold subducted slabs, the V_Φ of F-bearing Shy-B is almost consistent with the breakdown products. The solubility of H in bridgmanite ranges from 0.1 to 0.62 wt% in presence of Al, Fe and F (Yoshino and Jaseem, 2018; Fu et al., 2019). Hence, bridgmanite has the ability to accommodate high amounts of H which originate from decomposition of Shy-B. Due to this consumption, partial melt formation by Shy-B breakdown in uppermost lower mantle is very unlikely. The downward flow of transition zone materials, at least contain ~6.2 wt% H, may be the primary contributor (Schmandt et al., 2014).

Acknowledgments

X. Wu acknowledges financial support from the National Science Foundation of China (41473056 and 41827802). This work is supported by a joint research program at the Institute for Planetary Materials, Okayama University. We would like to thank Sergey Tkachev for gas loading the diamond anvil cells, Qian Zhang and Haipeng Song for experiment preparations. This work was performed at GeoSoilEnviroCARS, Advanced Photon Source (APS), Argonne National Laboratory (ANL). GeoSoilEnviroCARS operations are supported by the National Science Foundation-Earth Sciences (EAR-1634415) and the Department of Energy,

328 Geosciences (DE-FG02-94ER14466). APS is supported by DOE-BES, under Contract
329 No. DE-AC02-06CH11357. PX2 and the GSECARS/COMPRES gas loading system
330 are supported in part by COMPRES under NSF Cooperative Agreement
331 EAR-1661511. All the data to produce all the figures in this paper are available on
332 Zenodo (doi：10.5281/zenodo.3993846).
333

References:

Angel, R.J., Alvaro, M., & Gonzalez-Platas, J. (2014). EosFit7c and a Fortran module (library) for equation of state calculations. *Zeitschrift für Kristallographie - Crystalline Materials*, *229*, 405–419. doi:10.1515/zkri-2013-1711

Bercovici, D., & Karato, S.-I. (2003). Whole-mantle convection and the transition-zone water filter. *Nature*, *425*, 39–44. doi:10.1038/nature01918

Crichton, W.A., Ross, N.L., & Gasparik T. (1999). Equations of state of magnesium silicates anhydrous B and superhydrous B. *Physics and Chemistry of Minerals*, *26*, 570–575. doi:10.1007/s002690050220

Dalou, C., Koga, K.T., Shimizu, N., Boulon, J., & Devidal, J.-L. (2012). Experimental determination of F and Cl partitioning between lherzolite and basaltic melt. *Contributions to Mineralogy and Petrology*, *163*, 591–609. doi: 10.1007/s00410-011-0688-2

Dziewonski, A.M., & Anderson, D.L. 1981. Preliminary reference Earth model. *Physics of the Earth and Planetary Interiors*, *25*, 297–356. doi:10.1016/0031-9201(81)90046-7

Fei, Y., Ricolleau, A., Frank, M., Mibe, K., Shen, G., & Prakapenka, V. (2007). Toward an internally consistent pressure scale. *Proceedings of the National Academy of Sciences*, *104*, 9182–9186. doi:10.1073/pnas.0609013104

Fu, S.Y., Yang, J., Karato, S.-I., Vasiliev, A., Presniakov, M.Y., Gavrilliuk, A.G., et al. (2019). Water Concentration in Single-Crystal (Al,Fe)-Bearing Bridgmanite Grown From the Hydrous Melt: Implications for Dehydration Melting at the Topmost Lower Mantle. *Geophysical Research Letters*, *46*, 10346–10357. doi:10.1029/2019GL084630

Grützner, T., Klemme, S., Rohrbach, A., Gervasoni, F., & Berndt, J. (2018). The effect of fluorine on the stability of wadsleyite: implications for the nature and depths of the transition zone in the Earth's mantle. *Earth and Planetary Science Letters*, *482*, 236–244. doi:10.1016/j.epsl.2017.11.011

Grützner, T., Klemme, S., Rohrbach, A., Gervasoni, F., & Berndt, J. (2017b). The role of F-clinohumite in volatile recycling processes in subduction zones. *Geology*, *45*, 443–446. doi:10.1130/G38788.1

Grützner, T., Kohn, S.C., Bromiley, D.W., Rohrbach, A., Berndt, J., & Klemme, S. (2017a). The storage capacity of fluorine in olivine and pyroxene under upper mantle conditions. *Geochimica et Cosmochimica Acta*, *208*, 160–170. doi:10.1016/j.gca.2017.03.043

Hazen, M., Yang, H., Prewitt, C. T., & Gasparik, T. (1997). Crystal chemistry of superfluorous phase B ($Mg_{10}Si_3O_{14}F_4$): implications for the role of fluorine in the mantle. *American Mineralogist*, *82*, 647–650. doi: 10.2138/am-1997-5-626

Hirschmann M.M. (2006). Water, melting, and the deep earth H_2O cycle. *Annual Review of Earth and Planetary Sciences*, *34*, 29–53. doi:10.1146/annurev.earth.34.031405.125211

Inoue, T. (1994). Effect of water on melting phase relations and melt composition in the system Mg_2SiO_4–$MgSiO_3$–H_2O up to 15 GPa. *Physics of the Earth and Planetary Interiors*, *85*, 237–263. doi:10.1016/0031-9201(94)90116-3

Inoue, T., Ueda, T., Higo, Y., Yamada, A., Irifune, T., & Funakoshi, K.I. (2006). High-pressure and high-temperature stability and equation of state of superhydrous phase B. In: Jacobsen, S.D., Lee, S. (Eds), Earth's Deep Water Cycle. AGU, Washington, D. C., pp. 147–157.

Irifune, T., & Ringwood, A.E. (1987). Phase transformations in a harzburgite composition to 26 GPa: Implications for dynamical behaviour of the subducting slab. *Earth and Planetary Science Letters*, *86*, 365–376. doi:10.1016/0012-821X(87)90233-0

Joachim, B., Pawley, A., Lyon, I.C., Marquardt, K., Henkel, T., Clay, P.L., et al. (2015). Experimental partitioning of F and Cl between olivine, orthopyroxene and silicate melts at Earth's mantle conditions. *Chemical Geology*, *416*, 65–78. doi:10.1016/j.chemgeo.2015.08.012

John, T., Scambelluri, M., Frische, M., Barnes, J.D., & Bach, W. (2011). Dehydration of subducting serpentinite: implications for halogen mobility in subduction zones

and the deep halogen cycle. *Earth and Planetary Science Letters*, *308*, 65–76. doi:10.1016/j.epsl.2011.05.038

Kohlstedt, D., Keppler, H., & Rubie, D.C. (1996). Solubility of water in the α, β and γ phases of $(Mg,Fe)_2SiO_4$. *Contributions to Mineralogy and Petrology*, *123*, 345–357. doi:10.1007/s004100050161

Kudoh, Y., Nagase, T., Ohta, S., Sasaki, S., Kanzaki, M., & Tanaka, M. (1994). Crystal-structure and compressibility of superhydrous phase-B, $Mg_{20}Si_6H_8O_{36}$, paper presented at AIP Conf. Proc., Colorado Springs, Colo.

Kudoh, Y., Nagase, T., Sasaki, S., Tanaka, M., & Kanzaki, M. (1995). Phase F, a new hydrous magnesium silicate synthesized at 1000 °C and 17 GPa: crystal structure and estimated bulk modulus. *Physics and Chemistry of Minerals*, *22*, 295–299. doi:10.1007/s002690050078

Kuribayashi, T., Kudoh, Y., & Akizuki, M. (1998). Single-crystal X-ray diffraction and FTIR spectra of chondrodite, $Mg_5Si_2O_8(OH,F)_2$ under high pressure to 6.0 GPa. 17th General Meeting of the International Mineralogical Association, Toronto, A44

Li, X.Y., Mao, Z., Sun, N.Y., Liao, Y.F., Zhai, S.M., Wang, Y., et al. (2016). Elasticity of single-crystal superhydrous phase B at simultaneous high pressure-temperature conditions. *Geophysical Research Letters*, *43*, 8458–8465. doi:10.1002/2016GL070027

Li, Y., Jiang, H., & Yang, X. (2017). Fluorine follows water: Effect on electrical conductivity of silicate minerals by experimental constraints from phlogopite. *Geochimica et Cosmochimica Acta*, *217*, 16–27. doi:10.1016/j.gca.2017.08.020

Litasov, K.D., Ohtani, E., Ghosh, S., Nishihara, Y., Suzuki, A., & Funakoshi, K. (2007). Thermal equation of state of superhydrous phase B to 27 GPa and 1373 K. *Physics of the Earth and Planetary Interiors*, *164*, 142–160. doi:10.1016/j.pepi.2007.06.003

Liu, L.G., Lin, C.C., Mernagh, T.P., & Inoue, T. (2002). Raman spectra of phase C (superhydrous phase B) at various pressures and temperatures. *European Journal of Mineralogy*, *15*, 15–23. doi:10.1127/0935-1221/2002/0014-0015

McDonough, W. F., & Sun, S.-S. (1995). The composition of the Earth. *Chemical Geology*, *120*, 223–253. doi:10.1016/0009-2541(94)00140-4

Mookherjee, M., Speziale, S., Marquardt, H., Jahn, S., Wunser, B., Koch-Müller, K. et al. (2015). Equation of state and elasticity of the 3.65 Å phase: Implications for the X-discontinuity. *American Mineralogist*, *100*, 2199–2208. doi:10.2138/am-2015-5312

Mookherjee, M., & Tsuchiya, J. (2015). Elasticity of superhydrous phase, B, $Mg_{10}Si_3O_{14}(OH)_4$. *Physics of the Earth and Planetary Interiors*, *238*, 42–50. doi:10.1016/j.pepi.2014.10.010

Nishihara, Y., Takahashi, E., Matsukage, K., & Kikegawa, T. (2003). Thermal equation of state of omphacite. *American Mineralogist*, *88*, 80–86. doi:10.2138/am-2003-0110

Ohtani, E., Toma, M., Kubo, T., Kondo, T., & Kikegawa, T. (2003). In situ X-ray observation of decomposition of superhydrous phase B at high pressure and temperature. *Geophysical Research Letters*, *30*, 1029. doi:10.1029/2002GL015549

Pearson, D.G., Brenker, F.E., Nestola, F., McNeill, J., Nasdala, L., Hutchison, M.T., et al. (2014). Hydrous mantle transition zone indicated by ringwoodite included within diamond. *Nature*, *507*, 221–224. doi:10.1038/nature13080

Poswal, H.K., Sharma, S.M., & Sikka, S.K. (2010). Investigation of structure and hydrogen bonding of superhydrous phase B (HT) under pressure using first-principles density functional calculations. *High Pressure Research*, *30*, 198–206. doi:10.1080/08957950903503920

Qin, F., Wu, X., Zhang, D.Z., Qin, S., & Jacobsen, S.D. (2017). Thermal Equation of State of Natural Ti-Bearing Clinohumite. *Journal of Geophysical Research: Solid Earth*, *122*, 8943–8951. doi:10.1002/2017JB014827

448 Roberge, M., Bureau, H., Bolfan-Casanova, N., Frost, D.J., Raepsaet, C., Surble, S.,
449 et al. (2015). Is the transition zone a deep reservoir for fluorine? *Earth and*
450 *Planetary Science Letters*, 429, 25–32. doi:10.1016/j.epsl.2015.07.051
451 Rosa, A.D., Sanchez-Valle, C., Wang, J.Y., & Saikia, A. (2015). Elasticity of
452 superhydrous phase B, seismic anomalies in cold slabs and implications for deep
453 water transport. *Physics of the Earth and Planetary Interiors*, *243*, 30–43.
454 doi:10.1016/j.pepi.2015.03.009
455 Ross, N.L., & Crichton, W.A. (2001). Compression of synthetic hydroxylclinohumite
456 [$Mg_9Si_4O_{16}(OH)_2$] and hydroxylchondrodite [$Mg_5Si_2O_8(OH)_2$]. *American*
457 *Mineralogist*, *86*, 990–996. doi:10.2138/am-2001-8-905
458 Saal A.E., Hauri E.H., Langmuir C.H., & Perfit M.R. (2002). Vapour undersaturation
459 in primitive mid-ocean-ridge basalt and the volatile content of Earth's upper
460 mantle. *Nature*, *419*, 451–455. doi:10.1038/nature01073
461 Sanchez-Valle, C., Sinogeikin, S.V., Smyth, J.R., & Bass, J.D. (2008). Sound
462 velocities and elasticity of DHMS phase A to high pressure and implications for
463 seismic velocities and anisotropy in subducted slab. *Physics of the Earth and*
464 *Planetary Interiors*, *170*, 229–239. doi:10.1016/j.pepi.2008.07.015
465 Schilling J.-G., Bergeron M.B., & Evans R. (1980). Halogens in the mantle beneath
466 the North Atlantic. *Philosophical Transactions - Mathematical, Physical, and*
467 *Engineering Sciences*, *297*, 147–178.
468 Schmandt, B., Jacobsen, S.D., Becker, T.W., Liu, Z., & Dueker, K.G. (2014).
469 Dehydration melting at the top of the lower mantle. *Science*, *344*, 1265–1268.
470 doi:10.1126/science.1253358
471 Shieh, S.R., Mao, H.K., Hemley, R.J., & Ming, L.C. (2000). In situ X-ray diffraction
472 studies of dense hydrous magnesium silicates at mantle conditions. *Earth and*
473 *Planetary Science Letters*, *177*, 69–80. doi:10.1016/S0012-821X(00)00033-9
474 Smyth, J.R. (1987). β-Mg_2SiO_4: a potential host for water in the mantle? *American*
475 *Mineralogist*, *72*, 1051–1055.

476 Straub, S.M., & Layne, G.D. (2003). The systematics of chlorine, fluorine, and water
477 in Izu arc front volcanic rocks: implications for volatile recycling in subduction
478 zones. *Geochimica et Cosmochimica Acta*, *67*, 4179–4203.
479 doi:10.1016/S0016-7037(03)00307-7
480 Tsuchiya, J., & Mookherjee, M. (2015). Crystal structure, equation of state, and
481 elasticity of phase H ($MgSiO_4H_2$) at Earth's lower mantle pressures. *Scientific*
482 *Report*, *5*, 15534. doi:10.1038/srep15534
483 Ulian, G., & Valdrè, G. (2017). Effects of fluorine content on the elastic behavior of
484 topaz [$Al_2SiO_4(F,OH)_2$]. *American Mineralogist*, *102*, 347–356.
485 doi:10.2138/am-2017-5668
486 Wu, X., Wu, Y., Lin, J. F., Liu, J., Mao, Z., Guo, X., et al. (2016). Two-stage spin
487 transition of iron in FeAl-bearing phase D at lower mantle. *Journal of*
488 *Geophysical Research: Solid Earth*, *121*, 6411–6420. doi:
489 10.1002/2016JB013209
490 Yang, D., Wang, W.Z., & Wu, Z.Q. (2017). Elasticity of superhydrous phase B at the
491 mantle temperatures and pressures: Implications for 800 km discontinuity and
492 water flow into the lower mantle. *Journal of Geophysical Research: Solid Earth*,
493 *122*, 5026–5037. doi:10.1002/2017JB014319
494 Yoshino. T., & Jaseem, V. (2018). Solubility in bridgmanite: A potential fluorine
495 reservoir in the Earth's mantle. *Earth and Planetary Science Letters*, *504*, 106–
496 114. doi: 10.1016/j.epsl.2018.10.009
497 Zhang, D.Z., Dera, P., Eng, P.J., Stubbs, J.E., Zhang, J.S., Prakapenka, V.B. et al.
498 (2017). High pressure single crystal diffraction at PX^2. *Jove-Journal of*
499 *Visualized Experiments*, *119*, e54660. doi: 10.3791/54660